High-Order Synchrosqueezing Transform for Multicomponent Signals Analysis-With an Application to Gravitational-Wave Signal

Duong-Hung Pham, Sylvain Meignen

High-Order Synchrosqueezing Transform for Multicomponent Signals Analysis - With an Application to Gravitational-Wave Signal

Duong-Hung Pham, and Sylvain Meignen.

Abstract

This study puts forward a generalization of the short-time Fourier-based Synchrosqueezing Transform using a new local estimate of instantaneous frequency. Such a technique enables not only to achieve a highly concentrated time-frequency representation for a wide variety of AM-FM multicomponent signals but also to reconstruct their modes with a high accuracy. Numerical investigation on synthetic and gravitational-wave signals shows the efficiency of this new approach.

Index Terms

Time-frequency, reassignment, synchrosqueezing, AM/FM, multicomponent signals.

I. Introduction

Many signals such as audio signals (music, speech), medical data (electrocardiogram, thoracic and abdominal movement signals), can be modeled as a superposition of amplitude- and frequency-modulated (AM-FM) modes [1]–[3], called multicomponent signals (MCS). Linear techniques as for instance continuous wavelet transforms (CWT) and short-time Fourier transform (STFT) are often utilized to characterize such signals in the time-frequency (TF) plane. However, they all share the same limitation, known as the "uncertainty principle", stipulating that one cannot localize a signal with arbitrary precision both in time and frequency. Many efforts were made to cope with this issue and, in particular, a general methodology to sharpen TF representation, called "reassignment" method (RM) was proposed. This was

D-H Pham and S. Meignen are with the Jean Kuntzmann Laboratory, University of Grenoble-Alpes, and CNRS, Grenoble 38041, France (email:duong-hung.pham@imag.fr and sylvain.meignen@imag.fr). The authors acknowledge the support of the French Agence Nationale de la Recherche (ANR) under reference ANR-13- BS03-0002-01 (ASTRES)

first introduced in [4], in a somehow restricted framework, and then further developed in [5], as a post-processing technique. The main problem associated with RM is that the reassigned transform is no longer invertible and does not allow for mode reconstruction.

In the context of audio signal analysis [6], Daubechies and Maes proposed another phase-based technique, called "SynchroSqueezing Transform" (SST), whose theoretical analysis followed in [7]. Its purpose is relatively similar to that of RM, i.e. to sharpen the time-scale (TS) representation given by CWT, with the additional advantage of allowing for mode retrieval. Using the principle of wavelet-based SST (WSST), Thakur and Wu proposed an extension of SST to the TF representation given by STFT (FSST) [8], which was then proven to be robust to small bounded perturbations and noise [9]. Nevertheless, the applicability of SST is somewhat hindered by the requirement of weak frequency modulation hypothesis for the modes constituting the signal. In contrast, most real signals are made up of very strongly modulated AM-FM modes, as for instance chirps involved in radar [10], speech processing [11], or gravitational waves [12], [13]. In this regard, a recent adaptation of FSST to the context of strongly modulated modes was introduced in [14], and further mathematically analyzed in [15]. Unfortunately, the aforementioned technique was proven to only provide an ideal invertible TF representation for linear chirps with Gaussian modulated amplitudes, which is still restrictive.

In this paper, we propose to improve existing STFT-based SSTs by computing more accurate estimates of the instantaneous frequencies of the modes making up the signal, using higher order approximations both for the amplitude and phase. This results in perfect concentration and reconstruction for a wider variety of AM-FM modes than what was possible up to now with synchrosqueezing techniques.

This paper is structured as follows: we recall some fundamental notation and definitions on Fourier Transform (FT), STFT and MCS in Section II-A, and introduce FSST with its extension, the second-order FSST (FSST2) respectively in Sections II-B and II-C. We then present the proposed generalization, called *higher-order synchrosqueezing transform* in Section III. Finally, the numerical simulations of Section IV demonstrate the interest of our technique on both simulated signals and a gravitational-wave signal.

II. Background to FSST

Before going in detail into the principle of FSST, the following section presents several notation that will be used in the sequel.

A. Basic Notation and Definitions

The Fourier transform (FT) of a given signal $f \in L^1(\mathbb{R})$ is defined as:

$$\hat{f}(\eta) = \int_{\mathbb{R}} f(t) e^{-i2\pi\eta t} dt. \tag{1}$$

If $\hat{f}$ is also integrable, f can be reconstructed through:

$$f(t) = \int_{\mathbb{R}} \hat{f}(\eta) e^{i2\pi\eta t} d\eta. \tag{2}$$

It is well known that time- or frequency-domain representation alone is not appropriate to describe non-stationary signals whose frequencies have a temporal localization. The short-time Fourier transform (STFT) was thus introduced for that purpose, and is defined as follows: given a signal $f \in L^1(\mathbb{R})$ and a window g in the Schwartz class, the space of smooth functions with fast decaying derivatives of any order, the (modified) STFT of f is defined by:

$$V_f^g(t,\eta) = \int_{\mathbb{R}} f(\tau) g^*(\tau - t) e^{-2i\pi\eta(\tau - t)} d\tau, \tag{3}$$

where g^* is the complex conjugate of g, and then the spectrogram corresponds to $|V_f^g(t,\eta)|^2$. Furthermore, the original signal f can be retrieved from its STFT through the following synthesis formula, on condition that g does not vanish and is continuous at 0:

$$f(t) = \frac{1}{g^*(0)} \int_{\mathbb{R}} V_f^g(t,\eta) d\eta. \tag{4}$$

If f is analytic, i.e. $\eta \leq 0$ then $\hat{f}(\eta) = 0$, the integral in (4) only takes place on $\mathbb{R}_+$.

In the sequel, we will intensively study multicomponent signals (MCS) defined as a superposition of AM-FM components or modes:

$$f(t) = \sum_{k=1}^{K} f_k(t) \quad \textit{with} \quad f_k(t) = A_k(t) e^{i2\pi\phi_k(t)}, \tag{5}$$

for some finite $K \in \mathbb{N}$, $A_k(t)$ and $\phi_k(t)$ are respectively instantaneous amplitude (IA) and phase (IP) functions satisfying: $A_k(t) > 0, \phi_k'(t) > 0$ and $\phi_{k+1}'(t) > \phi_k'(t)$ for all t where $\phi_k'(t)$ is referred to as the instantaneous frequency (IF) of mode f_k at time t. Such a signal is fully described by its ideal TF (ITF) representation defined as:

$$\mathrm{TI}_f(t,\omega) = \sum_{k=1}^{K} A_k(t) \delta\left(\omega - \phi_k'(t)\right), \tag{6}$$

where δ denotes the Dirac distribution.

B. STFT-based SST (FSST)

The key idea of STFT-based SST (FSST) is to sharpen the "blurred" STFT representation of f by using the following IF estimate at time t and frequency η:

$$\hat{\omega}_f(t,\eta) = \frac{1}{2\pi} \partial_t \mathrm{arg}\left\{V_f^g(t,\eta)\right\} = \Re\left\{\frac{\partial_t V_f^g(t,\eta)}{2i\pi V_f^g(t,\eta)}\right\}, \tag{7}$$

where $\arg\{Z\}$ and $\Re\{Z\}$ stand for the argument and real part of complex number Z, respectively, and ∂_t is the partial derivative with respect to t.

Indeed, $V_f^g(t,\eta)$ is reassigned to a new position $(t, \hat{\omega}_f(t,\eta))$ using the synchrosqueezing operator defined as follows:

$$T_f^{g,\gamma}(t,\omega) = \frac{1}{g^*(0)} \int_{\{\eta, |V_f^g(t,\eta)|>\gamma\}} V_f^g(t,\eta)\delta\left(\omega - \hat{\omega}_f(t,\eta)\right) d\eta, \tag{8}$$

where γ is some threshold.

Since its coefficients are reassigned along the "frequency" axis, FSST preserves the causality property, thus making the k^{th} mode approximately reconstructed by integrating $T_f^{g,\gamma}(t,\eta)$ in the vicinity of the corresponding ridge $(t, \phi_k'(t))$:

$$f_k(t) \approx \int_{\{\omega, |\omega - \varphi_k(t)|<d\}} T_f^{g,\gamma}(t,\omega) d\omega, \tag{9}$$

where $\varphi_k(t)$ is an estimate of $\phi_k'(t)$. Parameter d enables to compensate for both the inaccurate approximation $\varphi_k(t)$ of $\phi_k'(t)$ and the error made by estimating the IF by means of $\hat{\omega}_f(t,\eta)$. It is worth noting here that the approximation $\varphi_k(t)$ must be computed before retrieving mode f_k. For that purpose, a commonly used technique is based on ridge extraction assuming $T_f^{g,\gamma}$ and K are known [7], [16]. This technique initially proposed by Carmona et *al.* [17] relies on the minimization of the following energy functional:

$$E_f(\varphi) = \sum_{k=1}^{K} - \int_{\mathbb{R}} |T_f^{g,\gamma}(t,\varphi_k(t))|^2 dt + \int_{\mathbb{R}} \lambda \varphi_k'(t)^2 + \beta \varphi_k''(t)^2 dt, \tag{10}$$

where λ and β are chosen regularization parameters such that the trade-off between smoothness of φ_k and energy is maximized. In practice, this energy functional is hard to implement because of its non-convexity, and so one should find tricks to avoid local minima as much as possible, as for example using a simulated annealing algorithm proposed in [17]. A recent algorithm introduced in [9], and used in this paper, determines the ridge associated with the corresponding mode thanks to a forward/backward approach for different initializations. Furthermore, a detailed study on the influence of the regularization parameters, introduced recently in [18], shows that they should not be used in (10) since they bring no improvement in term of accuracy of ridge estimation.

Finally, a very important aspect of FSST is that it is developed in a solid mathematical framework. Indeed, assume the modes of an MCS satisfy the following definition:

Definition II.1. *Let $\epsilon > 0$ and $\mathcal{B}_{\varepsilon,\Delta}$ be the class of MCS such that for all k, $A_k \in C^1(\mathbb{R}) \bigcap L^\infty(\mathbb{R})$, $\phi_k \in C^2(\mathbb{R})$, $supp_t \phi_k'(t) < \infty$, and for $\forall t$, $A_k(t) > 0$, $\phi_k'(t) > 0$ satisfy two hypotheses:*

- *H1) f_ks have weak frequency modulation, i.e. $\exists \varepsilon$ small s.t.: $|A_k'(t)| \leq \varepsilon$ and $|\phi_k''(t)| \leq \varepsilon$ for $\forall t$.*

- *H2) all f_ks are well separated in frequency, i.e. $|\phi'_{k+1}(t) - \phi'_k(t)| \geq 2\Delta$ for $\forall t$ and $\forall k \in \{1, ..., K\}$, where Δ is called the separation parameter.*

Then, it was proven in [15] that the synchrosqueezing operator $T_f^{g,\gamma}$ is concentrated in narrow bands around the curves $(t, \phi'_k(t))$ in the TF plane and the modes f_ks can be reconstructed from $T_f^{g,\gamma}(t, \omega)$ with a reasonably high accuracy.

C. Second Order STFT-based SST (FSST2)

Although FSST proves to be an efficient solution for enhancing TF representations, its application is restricted to a class of MCS composed of slightly perturbed pure harmonic modes. To overcome this limitation, a recent extension of FSST was introduced based on a more accurate IF estimate, which is then used to define an improved synchrosqueezing operator $T_{2,f}^{g,\gamma}(t, \eta)$, called second-order STFT-based synchrosqueezing transform (FSST2) [14], [15].

More precisely, a second-order local modulation operator is first defined and then used to compute the new IF estimate. This modulation operator corresponds to the ratio of the first-order derivatives, with respect to t, of the reassignment operators, as explained in the following:

Proposition II.1. *Given a signal $f \in L^2(\mathbb{R})$, the complex reassignment operators $\tilde{\omega}_f(t, \eta)$ and $\tilde{\tau}_f(t, \eta)$ are respectively defined for any (t, η) s.t. $V_f^g(t, \eta) \neq 0$ as:*

$$\begin{aligned} \tilde{\omega}_f(t, \eta) &= \frac{\partial_t V_f^g(t, \eta)}{2i\pi V_f^g(t, \eta)} \\ \tilde{\tau}_f(t, \eta) &= t - \frac{\partial_\eta V_f^g(t, \eta)}{2i\pi V_f^g(t, \eta)}. \end{aligned} \tag{11}$$

Then, the second-order local complex modulation operator $\tilde{q}_{t,f}(t, \eta)$ is defined by:

$$\tilde{q}_{t,f}(t, \eta) = \frac{\partial_t \tilde{\omega}_f(t, \eta)}{\partial_t \tilde{\tau}_f(t, \eta)} \qquad \textit{whenever } \partial_t \tilde{\tau}_f(t, \eta) \neq 0. \tag{12}$$

In that case, the definition of the improved IF estimate associated with the TF representation given by STFT is derived as:

Definition II.2. *Let $f \in L^2(\mathbb{R})$, the second-order local complex IF estimate of f is defined as:*

$$\tilde{\omega}_{t,f}^{[2]}(t, \eta) = \begin{cases} \tilde{\omega}_f(t, \eta) + \tilde{q}_{t,f}(t, \eta)(t - \tilde{\tau}_f(t, \eta)) & \textit{if } \partial_t \tilde{\tau}_f \neq 0 \\ \tilde{\omega}_f(t, \eta) & \textit{otherwise.} \end{cases}$$

Then, its real part $\hat{\omega}_{t,f}^{[2]}(t, \eta) = \Re\{\tilde{\omega}_{t,f}^{[2]}(t, \eta)\}$ is the desired IF estimate.

It was demonstrated in [14] that $\Re\{\tilde{q}_{t,f}(t,\eta)\} = \phi''(t)$ when f is a Gaussian modulated linear chirp, i.e. $f(t) = A(t)e^{i2\pi\phi(t)}$ where both $\log(A(t))$ and $\phi(t)$ are quadratic. Also, $\Re\{\tilde{\omega}^{[2]}_{t,f}(t,\eta)\}$ is an exact estimate of $\phi'(t)$ for this kind of signals. For a more general mode with Gaussian amplitude, its IF can be estimated by $\Re\{\tilde{\omega}^{[2]}_{t,f}(t,\eta)\}$, in which the estimation error only involves the derivatives of the phase with orders larger than 3. Furthermore, $\tilde{\omega}_f$, $\tilde{\tau}_f$ and $\tilde{q}_{t,f}$ can be computed by means of only five STFTs as follows:

Proposition II.2. *For a signal $f \in L^2(\mathbb{R})$, the expressions $\tilde{\omega}_f$, $\tilde{\tau}_f$ and $\tilde{q}_{t,f}$ can be written as:*

$$\tilde{\omega}_f = \eta - \frac{1}{i2\pi}\frac{V_f^{g'}}{V_f^g} \tag{13}$$

$$\tilde{\tau}_f = t + \frac{V_f^{tg}}{V_f^g} \tag{14}$$

$$\tilde{q}_{t,f} = \frac{1}{i2\pi}\frac{V_f^{g''}V_f^g - \left(V_f^{g'}\right)^2}{V_f^{tg}V_f^{g'} - V_f^{tg'}V_f^g}, \tag{15}$$

where V_f^g denotes $V_f^g(t,\eta)$ and $V_f^{g'}, V_f^{tg}, V_f^{g''}, V_f^{tg'}$ are respectively STFTs of f computed with windows $t \mapsto g'(t), tg(t), g''(t)$ and $tg'(t)$.

The second-order FSST (FSST2) is then defined by simply replacing $\hat{\omega}_f(t,\eta)$ by $\hat{\omega}^{[2]}_{t,f}(t,\eta)$ in (8):

$$T^{g,\gamma}_{2,f}(t,\omega) = \frac{1}{g^*(0)}\int_{\{\eta,|V_f^g(t,\eta)|>\gamma\}} V_f^g(t,\eta)\delta\left(\omega - \hat{\omega}^{[2]}_{t,f}(t,\eta)\right)d\eta.$$

Mode f_k is finally retrieved by replacing $T^{g,\gamma}_f(t,\omega)$ by $T^{g,\gamma}_{2,f}(t,\omega)$ in (9). Note that the theoretical foundation to support FSST2 has just been proposed in [15].

Remark. By using partial derivatives with respect to η instead of t, a new second-order local modulation operator $\tilde{q}_{\eta,f}(t,\eta)$ showing the same properties as those of $\tilde{q}_{t,f}(t,\eta)$ can be obtained as follows:

Definition II.3. *Given a signal $f \in L^2(\mathbb{R})$, the second-order local complex modulation operator $\tilde{q}_{\eta,f}$ is defined by:*

$$\tilde{q}_{\eta,f}(t,\eta) = \frac{\partial_\eta\tilde{\omega}_f(t,\eta)}{\partial_\eta\tilde{\tau}_f(t,\eta)} \qquad \textit{whenever } \partial_\eta\tilde{\tau}_f(t,\eta) \neq 0, \tag{16}$$

where $\tilde{\omega}_f(t,\eta)$ and $\tilde{\tau}_f(t,\eta)$ are respectively defined in (11).

The next proposition shows that this new operator also leads to a perfect estimate of the frequency modulation for a Gaussian modulated linear chirp.

Proposition II.3. *If $f(t) = A(t)e^{i2\pi\phi(t)}$ is a Gaussian modulated linear chirp, then $\Re\{\tilde{q}_{\eta,f}(t,\eta)\} = \phi''(t)$.*

Proof: Let us consider a mode $f(\tau) = A(\tau)e^{i2\pi\phi(\tau)}$ where $\log(A(\tau))$ and $\phi(\tau)$ are quadratic functions described by:

$$\log(A(\tau)) = \sum_{k=0}^{2} \frac{\alpha_k}{k!}\tau^k \quad \text{and} \quad \phi(\tau) = \sum_{k=0}^{2} \frac{\beta_k}{k!}\tau^k,$$

with $\alpha_k, \beta_k \in \mathbb{R}$. The STFT of this mode with any window g, at time t and frequency η, can be written as:

$$\begin{aligned} V_f^g(t,\eta) &= \int_{\mathbb{R}} f(\tau+t)g(\tau)e^{-i2\pi\eta\tau}d\tau \\ &= \int_{\mathbb{R}} \exp\left(\sum_{k=0}^{2} \frac{1}{k!}\left(\alpha_k + i2\pi\beta_k\right)(\tau+t)^k\right) g(\tau)e^{-i2\pi\eta\tau}d\tau. \end{aligned}$$

By taking the partial derivative of $V_f^g(t,\eta)$ with respect t, and then dividing by $i2\pi V_f^g(t,\eta)$, the local IF estimate $\tilde{\omega}_f(t,\eta)$ defined in (11) can be obtained for $V_f^g(t,\eta) \neq 0$:

$$\tilde{\omega}_f(t,\eta) = \sum_{k=1}^{2}\left(\frac{1}{i2\pi}\alpha_k + \beta_k\right)t^{k-1} + \left(\frac{1}{i2\pi}\alpha_2 + \beta_2\right)\frac{V_f^{tg}(t,\eta)}{V_f^g(t,\eta)}. \tag{17}$$

Then, taking the partial derivative of (17) with respect to η and recalling from Proposition II.2 that $\dfrac{V_f^{tg}(t,\eta)}{V_f^g(t,\eta)} = \tilde{\tau}_f(t,\eta) - t$, we get the following expression:

$$\partial_\eta\tilde{\omega}_f(t,\eta) = \left(\frac{1}{i2\pi}\alpha_2 + \beta_2\right)\partial_\eta\tilde{\tau}_f(t,\eta). \tag{18}$$

Setting $\tilde{q}_{\eta,f}(t,\eta) = \dfrac{\partial_\eta\tilde{\omega}_f(t,\eta)}{\partial_\eta\tilde{\tau}_f(t,\eta)}$ assuming $\partial_\eta\tilde{\tau}_f(t,\eta) \neq 0$ and noting that $\beta_2 = \phi''(t)$, ends the proof. ■

From (17) and (18), we also have the following result:

$$\begin{aligned} \phi'(t) &= \beta_1 + \beta_2 t \\ &= \Re\left\{\tilde{\omega}_f(t,\eta) - \left(\frac{1}{i2\pi}\alpha_2 + \beta_2\right)\left(\tilde{\tau}_f(t,\eta) - t\right)\right\} \\ &= \Re\left\{\tilde{\omega}_f(t,\eta) + \tilde{q}_{\eta,f}(t,\eta)(t - \tilde{\tau}_f(t,\eta))\right\}. \end{aligned} \tag{19}$$

Putting $\tilde{\omega}_{\eta,f}^{[2]}(t,\eta) = \tilde{\omega}_f(t,\eta) + \tilde{q}_{\eta,f}(t,\eta)(t - \tilde{\tau}_f(t,\eta))$, it follows that $\phi'(t) = \Re\left\{\tilde{\omega}_{\eta,f}^{[2]}(t,\eta)\right\}$. Thus, a new IF estimate having the same properties as $\tilde{\omega}_{t,f}^{[2]}(t,\eta)$ is introduced as follows:

Definition II.4. *Let $f \in L^2(\mathbb{R})$, the second-order local complex IF estimate of signal f is defined by:*

$$\tilde{\omega}_{\eta,f}^{[2]}(t,\eta) = \begin{cases} \tilde{\omega}_f(t,\eta) + \tilde{q}_{\eta,f}(t,\eta)(t - \tilde{\tau}_f(t,\eta)) & \text{if } \partial_\eta\tilde{\tau}_f(t,\eta) \neq 0 \\ \tilde{\omega}_f(t,\eta) & \text{otherwise.} \end{cases}$$

Then, its real part $\hat{\omega}_{\eta,f}^{[2]}(t,\eta) = \Re\{\tilde{\omega}_{\eta,f}^{[2]}(t,\eta)\}$ is the desired IF estimate.

Note, finally, that:

Proposition II.4. *The second-order modulation operator $\tilde{q}_{\eta,f}(t,\eta)$ can be computed by:*

$$\tilde{q}_{\eta,f} = \frac{1}{i2\pi}\frac{\left(V_f^g\right)^2 + V_f^g V_f^{tg'} - V_f^{g'} V_f^{tg}}{V_f^g V_f^{t^2 g} - \left(V_f^{tg}\right)^2}, \tag{20}$$

where $V_f^{t^2 g}$ is the STFT of the signal f computed with window $t \mapsto t^2 g(t)$.

Proof: By computing the partial derivatives of $\tilde{\omega}_f(t,\eta)$ and $\tilde{\tau}_f(t,\eta)$ with respect to η in the expressions given in Proposition II.2, and then using formula $\partial_\eta V_f^g(t,\eta) = -i2\pi V_f^{tg}(t,\eta)$, the expression for $\tilde{q}_{\eta,f}$ follows. ■

III. Higher Order Synchrosqueezing Transform

Despite FSST2 definitely improves the concentration of TF representation, it is only demonstrated to work well on perturbed linear chirps with Gaussian modulated amplitudes. To handle signals containing more general types of AM-FM modes having non-negligible $\phi_k^{(n)}(t)$ for $n \geq 3$, we are going to define new synchrosqueezing operators, based on approximation orders higher than three for both amplitude and phase.

A. Nth-order IF Estimate

The new IF estimate we define here is based on high order Taylor expansions of the amplitude and phase of a mode. For that purpose, let us first consider a mode defined as in the following:

Definition III.1. *Given a mode $f(\tau) = A(\tau)e^{i2\pi\phi(\tau)}$ in $L^2(\mathbb{R})$ with $A(\tau)$ (resp. $\phi(\tau)$) equal to its L^{th}-order (resp. N^{th}-order) Taylor expansion for τ close to t:*

$$\log(A(\tau)) = \sum_{k=0}^{L} \frac{[\log(A)]^{(k)}(t)}{k!}(\tau - t)^k$$

$$\phi(\tau) = \sum_{k=0}^{N} \frac{\phi^{(k)}(t)}{k!}(\tau - t)^k$$

where $Z^{(k)}(t)$ denotes the k^{th} derivative of Z evaluated at t.

A mode f defined as above, with $L \leq N$, can be written as:

$$f(\tau) = \exp\left(\sum_{k=0}^{N} \frac{1}{k!}\left([\log(A)]^{(k)}(t) + i2\pi\phi^{(k)}(t)\right)(\tau - t)^k\right),$$

since $[\log(A)]^{(k)}(t) = 0$ if $L+1 \leq k \leq N$. Consequently, the STFT of this mode at time t and frequency η can be written as:

$$\begin{aligned} V_f^g(t,\eta) &= \int_{\mathbb{R}} f(\tau+t)g(\tau)e^{-i2\pi\eta\tau}d\tau \\ &= \int_{\mathbb{R}} \exp\left(\sum_{k=0}^{N} \frac{1}{k!}\left([\log(A)]^{(k)}(t) + i2\pi\phi^{(k)}(t)\right)\tau^k\right) g(\tau)e^{-i2\pi\eta\tau}d\tau. \end{aligned}$$

By taking the partial derivative of $V_f^g(t,\eta)$ with respect to t and then dividing by $i2\pi V_f^g(t,\eta)$, the local IF estimate $\tilde{\omega}_f(t,\eta)$ defined in (11) can be written when $V_f^g(t,\eta) \neq 0$ as:

$$\begin{aligned} \tilde{\omega}_f(t,\eta) &= \sum_{k=1}^{N} r_k(t) \frac{V_f^{t^{k-1}g}(t,\eta)}{V_f^g(t,\eta)} \\ &= \frac{1}{i2\pi}[\log(A)]'(t) + \phi'(t) + \sum_{k=2}^{N} r_k(t) \frac{V_f^{t^{k-1}g}(t,\eta)}{V_f^g(t,\eta)}, \end{aligned} \tag{21}$$

where $r_k(t)$ are functions of t defined for $k = 1, \ldots, N$ as:

$$r_k(t) = \frac{1}{(k-1)!}\left(\frac{1}{i2\pi}[\log(A)]^{(k)}(t) + \phi^{(k)}(t)\right).$$

It is clear from (21) that, since $A(t)$ and $\phi(t)$ are real expressions, $\Re\{\tilde{\omega}_f(t,\eta)\} = \phi'(t)$ does not hold when the sum on the right hand side of (21) has a non-zero real part. As in the case of the Gaussian modulated linear chirp introduced before, to get the exact IF estimate for the studied signal, one needs to subtract $\Re\left\{\sum_{k=2}^{N} r_k(t) \frac{V_f^{t^{k-1}g}(t,\eta)}{V_f^g(t,\eta)}\right\}$ to $\Re\{\tilde{\omega}_f(t,\eta)\}$, for which $r_k(t)$, for all $k = 2, \ldots, N$, must be estimated.

For that purpose, inspired by our study of the Gaussian modulated linear chirp, we derive a frequency modulation operator $\tilde{q}_{\eta,f}^{[k,N]}$, equal to $r_k(t)$ when f satisfies Definition III.1, obtained by differentiating different STFTs with respect to η, as explained hereafter. Note that we choose to differentiate with respect to η rather than t because it leads to much simpler expressions, mainly as a result of the following formulae:

$$\begin{aligned} \partial_t V_f^g(t,\eta) &= i2\pi\eta V_f^g(t,\eta) - V_f^{g'}(t,\eta) \\ \partial_\eta V_f^g(t,\eta) &= -i2\pi V_f^{tg}(t,\eta). \end{aligned} \tag{22}$$

The different modulation operators $\tilde{q}_{\eta,f}^{[k,N]}$ for $k = 2, \ldots, N$ can then be derived recursively, as explained in the next proposition:

Proposition III.1. *Given a mode $f \in L^2(\mathbb{R})$ that satisfies Definition III.1 with $L \leq N$, the $N-1$ local modulation operators $\tilde{q}_{\eta,f}^{[k,N]}$ such that $\Re\left\{\tilde{q}_{\eta,f}^{[k,N]}(t,\eta)\right\} = \dfrac{\phi^{(k)}(t)}{(k-1)!}$, $k = 2,\ldots,N$, can be determined by:*

$$\tilde{q}_{\eta,f}^{[N,N]}(t,\eta) = y_N(t,\eta) \text{ and}$$

$$\tilde{q}_{\eta,f}^{[j,N]}(t,\eta) = y_j(t,\eta) - \sum_{k=j+1}^{N} x_{k,j}(t,\eta)\tilde{q}_{\eta,f}^{[k,N]}(t,\eta) \qquad \text{for } j = N-1, N-2, \ldots, 2,$$

where $y_j(t,\eta)$ and $x_{k,j}(t,\eta)$ are defined as follows. For any (t,η) s.t. $V_f^g(t,\eta) \neq 0$ and $\partial_\eta x_{j,j-1}(t,\eta) \neq 0$, we put:

$$\text{for } k = 1\ldots N, \quad y_1(t,\eta) = \tilde{\omega}_f(t,\eta) \text{ and } x_{k,1}(t,\eta) = \frac{V_f^{t^{k-1}g}(t,\eta)}{V_f^g(t,\eta)},$$

and then for $j = 2\ldots N$ and $k = j\ldots N$,

$$y_j(t,\eta) = \frac{\partial_\eta y_{j-1}(t,\eta)}{\partial_\eta x_{j,j-1}(t,\eta)} \text{ and } x_{k,j}(t,\eta) = \frac{\partial_\eta x_{k,j-1}(t,\eta)}{\partial_\eta x_{j,j-1}(t,\eta)}.$$

The proof of Proposition III.1 is given in Appendix A. Then, the definition of the N^{th}-order IF estimate follows:

Definition III.2. *Let $f \in L^2(\mathbb{R})$, the N^{th}-order local complex IF estimate $\tilde{\omega}_{\eta,f}^{[N]}$ at time t and frequency η is defined by:*

$$\tilde{\omega}_{\eta,f}^{[N]}(t,\eta) = \begin{cases} \tilde{\omega}_f(t,\eta) + \sum_{k=2}^{N} \tilde{q}_{\eta,f}^{[k,N]}(t,\eta)\left(-x_{k,1}(t,\eta)\right), & \text{if } V_f^g(t,\eta) \neq 0 \\ & \text{and } \partial_\eta x_{j,j-1}(t,\eta) \neq 0 \text{ for } j = 2\ldots N. \\ \tilde{\omega}_f(t,\eta) & \text{otherwise.} \end{cases}$$

Then, its real part $\hat{\omega}_{\eta,f}^{[N]}(t,\eta) = \Re\{\tilde{\omega}_{\eta,f}^{[N]}(t,\eta)\}$ is the desired IF estimate.

For this estimate, we have the following approximation result:

Proposition III.2. *Given a mode $f \in L^2(\mathbb{R})$ that satisfies Definition III.1 with $L \leq N$, then $\phi'(t) = \Re\left\{\tilde{\omega}_{\eta,f}^{[N]}(t,\eta)\right\}$.*

Proof: From (21), we have:

$$\begin{aligned}\phi'(t) &= \Re\left\{\tilde{\omega}_f(t,\eta) + \sum_{k=2}^{N} r_k(t)\left(-\frac{V_f^{t^{k-1}g}(t,\eta)}{V_f^{g}(t,\eta)}\right)\right\}\\ &= \Re\left\{\tilde{\omega}_f(t,\eta) + \sum_{k=2}^{N} r_k(t)\left(-x_{k,1}(t,\eta)\right)\right\}\\ &= \Re\left\{\tilde{\omega}_f(t,\eta) + \sum_{k=2}^{N} \tilde{q}_{\eta,f}^{[k,N]}(t,\eta)\left(-x_{k,1}(t,\eta)\right)\right\}. \end{aligned} \tag{23}$$

Let us put $\tilde{\omega}_{\eta,f}^{[N]}(t,\eta) = \tilde{\omega}_f(t,\eta) + \sum_{k=2}^{N} \tilde{q}_{\eta,f}^{[k,N]}(t,\eta)\left(-x_{k,1}(t,\eta)\right)$, we obtain $\phi'(t) = \Re\left\{\tilde{\omega}_{\eta,f}^{[N]}(t,\eta)\right\}$, which ends the proof. ■

B. Efficient Computation of Modulation Operators

The local modulation operators $\tilde{q}_{\eta,f}^{[k,N]}$ defined in Proposition III.1 should not be computed by approximating partial derivatives by means of discrete differentiation, since this would generate numerical instability especially in the presence of noise. Therefore, to deal with this issue, we remark that these modulation operators can instead be computed analytically as functions of different STFTs. This is illustrated for $N = 4$ through the following proposition:

Proposition III.3. *Let $f \in L^2(\mathbb{R})$, the modulation operators $\tilde{q}_{\eta,f}^{[k,N]}$ for $N = 4$ and $k = 2, 3, 4$ can be expressed as:*

$$\begin{aligned}\tilde{q}_{\eta,f}^{[4,4]} &= G_4\left(V_f^{t^{0\cdots6}g}, V_f^{t^{0\cdots3}g'}\right),\\ \tilde{q}_{\eta,f}^{[3,4]} &= G_3\left(V_f^{t^{0\cdots4}g}, V_f^{t^{0\cdots2}g'}\right) - \tilde{q}_{\eta,f}^{[4,4]} G_{3,4}\left(V_f^{t^{0\cdots5}g}\right),\\ \tilde{q}_{\eta,f}^{[2,4]} &= G_2\left(V_f^{t^{0\cdots2}g}, V_f^{t^{0\cdots1}g'}\right) - \tilde{q}_{\eta,f}^{[3,4]} G_{2,3}\left(V_f^{t^{0\cdots3}g}\right) - \tilde{q}_{\eta,f}^{[4,4]} G_{2,4}\left(V_f^{t^{0\cdots4}g}\right),\end{aligned}$$

where $G_k\left(V_f^{t^{0\cdots m}g}, V_f^{t^{0\cdots n}g'}\right)$ is a function of $V_f^{t^l g}$ for $l = 0, \ldots, m$ and $V_f^{t^l g'}$ for $l = 0, \ldots, n$ while $G_{k,j}\left(V_f^{t^{0\cdots m}g}\right)$ is associated with coefficient $\tilde{q}_{\eta,f}^{[j,N]}$ in the computation of $\tilde{q}_{\eta,f}^{[k,N]}$ for $k \neq j$.

Also, we recall that the fourth order IF estimate can be written as:

$$\tilde{\omega}_{\eta,f}^{[4]}(t,\eta) = \tilde{\omega}_f(t,\eta) + \tilde{q}_{\eta,f}^{[2,4]}(t,\eta)\left(-x_{2,1}(t,\eta)\right) + \tilde{q}_{\eta,f}^{[3,4]}(t,\eta)\left(-x_{3,1}(t,\eta)\right) + \tilde{q}_{\eta,f}^{[4,4]}(t,\eta)\left(-x_{4,1}(t,\eta)\right).$$

The proof of Proposition III.3 is available in Appendix B where explicit forms for G_k and $G_{k,j}$ are given.

Remark. We first note that when $N = 2$, i.e. by neglecting $\tilde{q}_{\eta,f}^{[3,4]}$ and $\tilde{q}_{\eta,f}^{[4,4]}$ corresponding to orders 3 and 4, the second-order IF estimate $\tilde{\omega}_{\eta,f}^{[2]}(t,\eta)$ defined in Proposition II.4 is found again. Secondly, it is

clear that the number of STFTs used to compute $\tilde{q}_{\eta,f}^{[4,4]}$ is 11, namely $V_f^{t^l g}$ for $l = 0, \ldots, 6$, and $V_f^{t^l g'}$ for $l = 0, \ldots, 3$. Finally, generalizing the procedure detailed in the proof of Proposition III.3 to any N, one obtains that $\tilde{q}_{\eta,f}^{[N,N]}$ can be computed by means of $3N-1$ STFTs, namely $V_f^{t^l g}$ for $l = 0, \ldots, 2N-2$, and $V_f^{t^l g'}$ for $l = 0, \ldots, N-1$.

C. Nth-order STFT-based SST (FSSTN)

As for FSST2, the N^{th}-order FSST (FSSTN) is defined by replacing $\hat{\omega}_f(t,\eta)$ by $\hat{\omega}_{\eta,f}^{[N]}(t,\eta)$ in (8):

Definition III.3. *Given $f \in L^2(\mathbb{R})$ and a real number $\gamma > 0$, one defines the FSSTN operator with threshold γ as:*

$$T_{N,f}^{g,\gamma}(t,\omega) = \frac{1}{g^*(0)} \int_{\{\eta, |V_f^g(t,\eta)|>\gamma\}} V_f^g(t,\eta)\delta\left(\omega - \hat{\omega}_{\eta,f}^{[N]}(t,\eta)\right) d\eta.$$

Finally, the modes of the MCS can be reconstructed by replacing $T_f^{g,\gamma}(t,\omega)$ by $T_{N,f}^{g,\gamma}(t,\omega)$ in (9).

IV. Numerical Analysis of the Behavior of STFT-based SST

This section presents numerical investigations to illustrate the improvements brought by our new technique in comparison with the standard reassignment method (RM) or existing STFT-based SSTs (FSST and FSST2) on both simulated and real signals. For that purpose, let us first consider a simulated MCS composed of two AM-FM components:

$$f(t) = f_1(t) + f_2(t) = A_1(t)e^{i2\pi\phi_1(t)} + A_2(t)e^{i2\pi\phi_2(t)},$$

with $A_k(t)$ and $\phi_k(t)$ defined on $[0,1]$, for $k = 1, 2$, by:

$$A_1(t) = \exp\left(2(1-t)^3 + t^4\right),\ A_2(t) = 1 + 5t^2 + 7(1-t)^6 \text{ and}$$

$$\phi_1(t) = 50t + 30t^3 - 20(1-t)^4,\ \phi_2(t) = 340t - 2\exp\left(-2(t-0.2)\right)\sin\left(14\pi(t-0.2)\right).$$

Note that f_1 is a polynomial chirp that satisfies Definition III.1 with $L = N = 4$, while f_2 is a damped-sine function containing very strong nonlinear sinusoidal frequency modulations and high-order polynomial amplitude modulations. In our simulations, f is sampled at a rate $M = 1024$ Hz on $[0,1]$. In Figures 1(a) and (b), we display the real part of f_1 and f_2 along with their amplitudes, and, in Figure 1 (c), the real part of f.

The STFT of f is then computed with the L^1-normalized Gaussian window $g(t) = \sigma^{-1}e^{-\pi\frac{t^2}{\sigma^2}}$, where σ is optimal in some sense as explained hereafter. One of the well-known issues regarding the use of STFT to analyze signals is the choice of an appropriate Gaussian window length to allow for a good trade-off between time and frequency localization. In the synchrosqueezing context, the choice of analysis window for the STFT has a strong impact on the accuracy of mode reconstruction: to use an

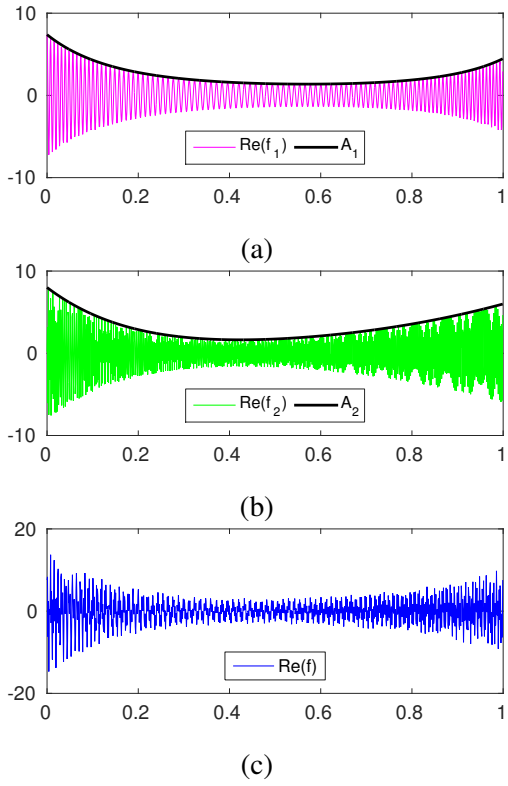

Fig. 1. (a) and (b): real part of f_1 and f_2 respectively with A_1 and A_2 superimposed; (c): real part of f.

inappropriate window may lead to the failure of ridge extraction and then of mode retrieval. To deal with this issue, a widely used approach is to measure the concentration of STFT which then allows us to pick the 'optimal' window length as the one associated with the most concentrated representation. For that purpose, a relevant work is [19], in which the concentration of the STFT is measured by means of Rényi entropy:

$$H_R(\sigma) = \frac{1}{1-\alpha} \log_2 \left(\frac{\int\int_{\mathbb{R}^2} |V_f^g(t,\eta)|^\alpha d\eta dt}{\int\int_{\mathbb{R}^2} |V_f^g(t,\eta)| d\eta dt} \right), \tag{24}$$

with integer orders $\alpha > 2$ being recommended. The larger the Rényi entropy, the less concentrated the STFT. The optimal window length parameter is thus determined as: $\sigma_{opt} = \arg\min_{\sigma} (H_R(\sigma))$. In Figure 2, we display the evolution of Rényi entropy $(\alpha = 3)$ with respect to σ for the signal f introduced above at different noise levels (noise-free, -5, 0, 5 dB), which leads to an optimal value in each case, relatively stable with the noise level.

Having determined the optimal σ, we display, in the noise-free context, the STFT of f on the left of Figure 3. Then, on the right of this figure, close-ups of the STFT itself are depicted, along with reassigned versions of STFT either given by the reassignment method (RM) or FSST and variants, all

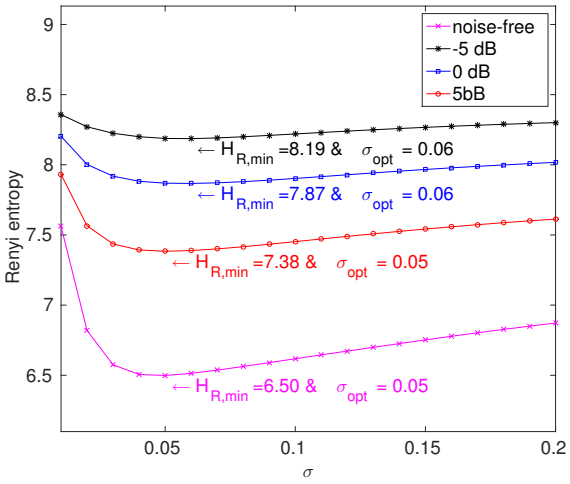

Fig. 2. Evolution of Rényi entropies (H_R) with respect to σ either in the noise-free, 5 dB, 0 dB or -5 dB cases.

mentioned in this paper. For the sake of consistency, we recall that RM corresponds to the reassignment of the spectrogram through [5]:

$$RM_f^g(t,\omega) = \int\int_{\mathbb{R}^2} |V_f^g(\tau,\eta)|^2 \delta\left(\omega - \hat{\omega}_f(\tau,\eta)\right) \delta\left(t - \hat{\tau}_f(\tau,\eta)\right) d\eta d\tau.$$

It behaves well with frequency modulation, but does not allow for mode reconstruction.

Analyzing these close-ups, we remark that, as expected, FSST2 leads to a relatively sharp TF representation for f_1, very similar to the one given by RM and much better than that corresponding to FSST. However, all these methods fail to reassign the STFT of f_2 correctly, especially where the IF of that mode has a non negligible curvature $\phi_2'''(t)$. In contrast, the TF reassignment of the STFT of f_2 provided by FSST3 or FSST4 is much sharper at these locations. Looking at what happens for mode f_1 also tells us that, FSST3 and FSST4 seems to behave very similarly to FSST2 or RM in terms of the sharpness of the representation. However, as we shall see later, the accuracy of the representation is improved by using one of the former two methods. Finally, note that since f_1 obeys Definition III.1, the IF estimate used in FSST4 is exact for that mode which results in perfect reassignment of the STFT.

For a better understanding of the performance improvements brought by the use of FSST3 and FSST4 over other studied methods, the following section first introduces a quantitative comparison of all these techniques from the angle of energy concentration of TF representations, and then a measure of their accuracy by means of the Earth mover's distance (EMD).

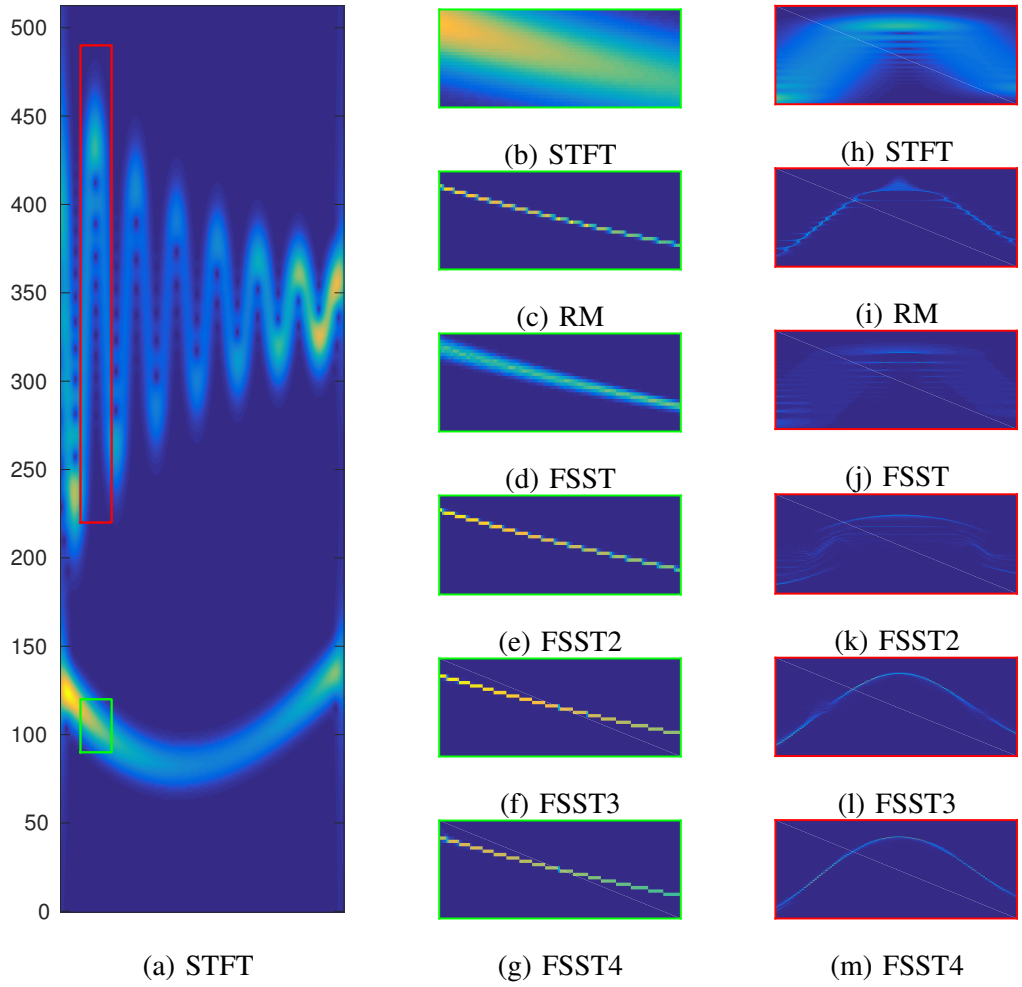

Fig. 3. *Right column panel*, (a): modulus of the STFT of f. *Middle column panel*, (b): STFT of a small TF patch corresponding to mode f_1 (delimited by green segments) extracted from (a); (c) RM carried out on the STFT shown in (b); from (d) to (g), same as (c) but using respectively FSST, FSST2, FSST3, FSST4. *Left column panel*, same as *middle column panel* but for f_2.

A. *Evaluation of TF Concentration*

To evaluate the performance of the different techniques regarding TF concentration, we first use a method introduced in [14]. The goal of this method is to measure the energy concentration by considering the proportion of the latter contained in the first nonzero coefficients associated with the highest amplitudes, which we call *normalized energy* in the sequel: the faster it increases towards 1 with the number of coefficients involved, the more concentrated the TF representation. In Figure 4 (a), we depict the normalized energy corresponding to the reassignment of the STFT of f_1 using different techniques, with respect to the number of coefficients kept divided by the length of f_1 (which corresponds to the sampling rate M in our case). Since we consider only one mode, a good representation has to

have its energy mostly contained in the first M coefficients, which correspond to abscissa 1 in the graph of Figure 4 (a). From this study and from this signal, it is hard to figure out the benefits of using FFST3 or FSST4 rather than the other two methods. The only thing one can check is that the energy is perfectly localized with FSST4 because f_1 obeys Definition III.1. The results of the same computation carried out for mode f_2 are displayed in Figure 4 (b), showing that the normalized energy is much more concentrated using FSST4 than the other methods, and that FSST3 also outperforms FSST2 and RM.

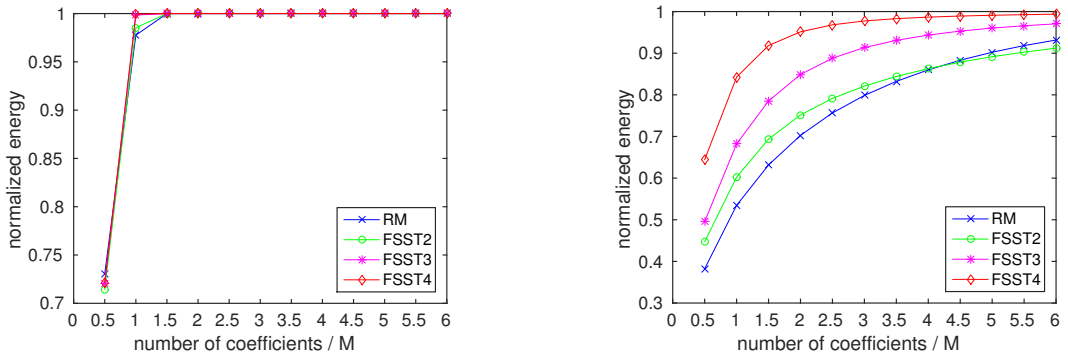

(a) (b)

Fig. 4. (a) Normalized energy as a function of the number of sorted associated coefficients for f_1; (b): same as (a) but for f_2.

To study the performance of the TF representations in the presence of noise, we consider a noisy signal, where the noise level is measured by the Signal-to-Noise Ratio (SNR):

$$\text{SNR}_{\text{intput}}[\text{dB}] = 20\log_{10}\frac{\text{std}(f)}{\text{std}(\zeta)}, \text{ where std is the standard deviation,} \tag{25}$$

and $\zeta(t)$ is the white Gaussian noise added. To compute the normalized energy as illustrated in Figure 4, though quite informative, does not deliver any insight into the accuracy of the reassigned transforms. The latter can alternatively be quantified by measuring the dissimilarity between the resultant TF representations and the ideal one by means of the Earth mover's distance (EMD), a procedure already used in the synchrosqueezing context in [20]. More precisely, this technique consists in computing the 1D EMD between the resultant TF representations and the ideal one, for each individual time t, and then take the average over all t to define the global EMD. A smaller EMD means a better TF representation concentration to the ground truth and less noise fluctuations. In Figures 5 (a) and (b), we display, respectively for f_1 and f_2, the evolution of EMD with respect to the noise level, for TF representations given either by FSST2, FSST3, FSST4 or RM. This study tells us that, at low noise level and for mode f_1, FSST3 and FSST4 are more accurate than the other studied methods. Note that this is something that could not be derived by the previous study on the normalized energy. The same

investigations but for mode f_2 confirms the interest of using FSST3 or FSST4 to reassign the STFT of a mode with IF exhibiting strong curvature. Note that the benefits of using the proposed new methods remain important even at high noise level.

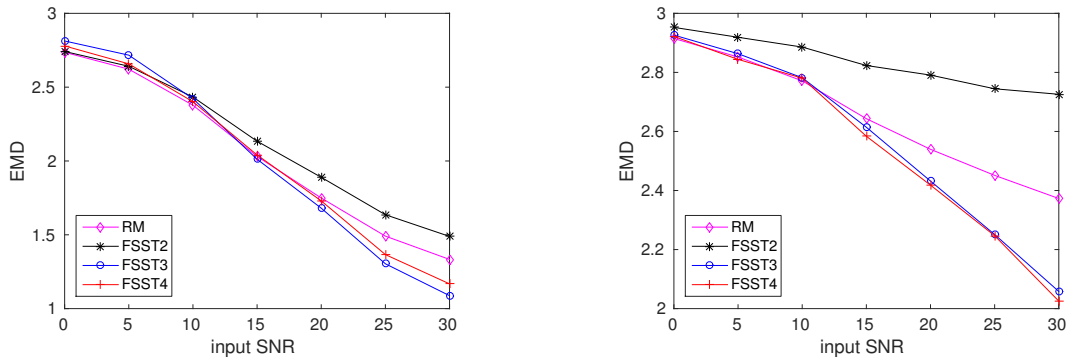

Fig. 5. (a): EMD corresponding to different TF representations of f_1 either given by RM, FSST2, FSST3 or FSST4; (b): same as (a) but for f_2.

B. Evaluation of Mode Reconstruction Performance

As discussed above, the variants of FSST proposed in this paper leading to significantly better TF representations, this should translate into better performance in terms of mode reconstruction. Let us first briefly recall the procedure to retrieve f_k from the TF representation of f given by the FSST of order N:

$$f_k(t) \approx \int_{\{\omega,|\omega-\varphi_k(t)|<d\}} T^{g,\gamma}_{N,f}(t,\omega)d\omega. \tag{26}$$

Note that $\varphi_k(t)$ is the estimate of $\phi'_k(t)$ given by the ridge detector (computed by minimizing energy (10) in which $T^{g,\gamma}_f$ is replaced by $T^{g,\gamma}_{N,f}$), and d is an integer parameter (because the frequency resolution is here associated with integer location) used to compensate for the inaccuracy of this estimation and also for the errors caused by approximating the IF by $\hat{\omega}^{[N]}_{\eta,f}(t,\eta)$. We first analyze the performance of the reconstruction procedure by considering the information on the ridge only, i.e. we take $d = 0$. For that purpose, we measure the output SNR, defined by $\text{SNR}_{\text{output}} = 20\log_{10}\dfrac{\|f\|_2}{\|f_r - f\|_2}$, where f_r is the reconstructed signal, and $\|.\|_2$ the l_2 norm. In Table I, we display this output SNR for modes f_1, f_2 and also for f, using either FSST2, FSST3 or FSST4 for mode reconstruction. The improvement brought by using FSST3 and FSST4 is clear and coherent with the previous study of the accuracy of the proposed new TF representations.

TABLE I

PERFORMANCE OF MODE RECONSTRUCTION IN THE NOISE-FREE CASE

	FSST2	**FSST3**	**FSST4**
Mode f_1	17.8	25.7	**28.8**
Mode f_2	1.73	3.62	**6.87**
MCS f	3.57	5.57	**8.82**

Parameter d also measures how well the TF representation is concentrated around the detected ridges: if the former is well concentrated, even if one uses a small d, the reconstruction results should be satisfactory. To measure this, we display in Figure 6, the output SNR corresponding to the reconstruction of f when d varies, and when the TF representation used for mode reconstruction is either FSST2, FSST3 and FSST4. From this Figure and for all tested methods, it is clear that a larger d means a more accurate reconstruction of the signal. Nevertheless, the accuracy the reconstruction using FSST2 seems to stagnate when some critical value for d is reached, which is not the case with the other two methods: the parameter d can only partly compensate for the inaccuracy of IF estimation. For that very reason, it is crucial to use the most accurate estimate as possible which again pleads in favor of FSST3 and FSST4.

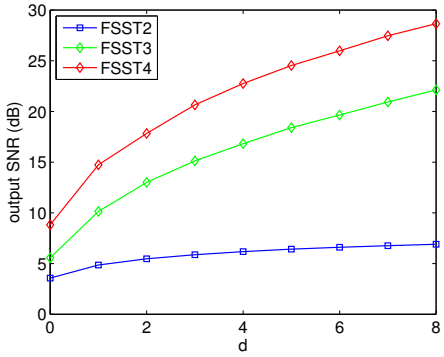

Fig. 6. Reconstruction accuracy measured in SNR with respect to d of the noise-free signal.

C. Application to Gravitational-wave Signal

In this section, we investigate the applicability of our new techniques for the analysis of a transient gravitational-wave signal, which was generated by the coalescence of two stellar-mass black holes. This event, called **GW150914**, was recently detected by the LIGO detector Hanford, Washington. Such a signal closely matches with waveform Albert Einstein predicted almost 100 years ago in his general relativity

theory for the inspiral, the merger of a pair of black holes and the ringdown of the resulting single black hole [13]. The observed signal has a length of 3441 samples in 0.21 seconds, which we pad with zeros to get a signal with 2^{12} samples, and the Gaussian window used in our simulations corresponds to $\sigma = 0.05$.

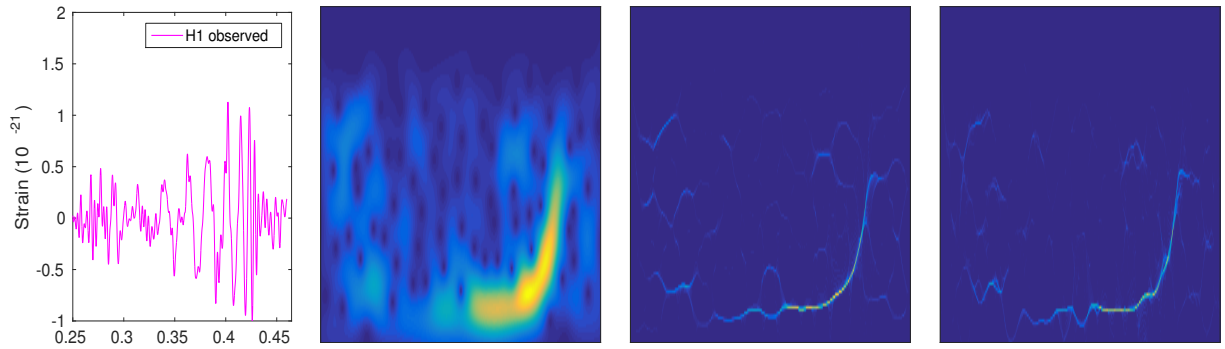

(a) (b) (c) (d)

Fig. 7. Illustration of the TF representations of the gravitational-wave event **GW150914**, (a): observed Hanford signal; (b): STFT; (c): FSST2; (d): FSST4.

We first display the gravitational-wave strain observed by the LIGO Hanford in Figure 7 (a), and the STFT, the reassigned transforms corresponding to FSST2 and FSST4 in Figure 7 (b), (c) and (d), respectively. The sharpened representations provided by FSST2 and FSST4 make the TF information more easily interpretable: as a matter of fact, the gravitational-wave signal consists of only one mode sweeping sharply upwards. However, the improvement brought by using high-order synchrosqueezing transform is not obvious at this point. Moving on to mode reconstruction, we perform ridge detection on each of the TF representations given by FSST2 and FSST4 and display the results in Figure 8 (a) and (b). We remark that FSST4 enables a better ridge detection of the three stages of the collision of two black-holes; especially the "ring down" one, which commences when the IF of the mode starts to decrease. This is associated with a sudden variation of the curvature of its IF which is better taken into account by FSST4. A consequence of this can be seen in Figure 8 (c) displaying the reconstructed mode using either FSST2 or FSST4, the latter leading to a much better reconstruction, very similar to the numerical relativity waveform obtained from an independent calculation [13]. This fact is finally reflected by Figure 8 (d) in which we display the residual errors (in l_2 norm) between the mode predicted by the numerical relativity and the one reconstructed from FSST2 or FSST4. This thus demonstrates the interest of the proposed new technique in real applications.

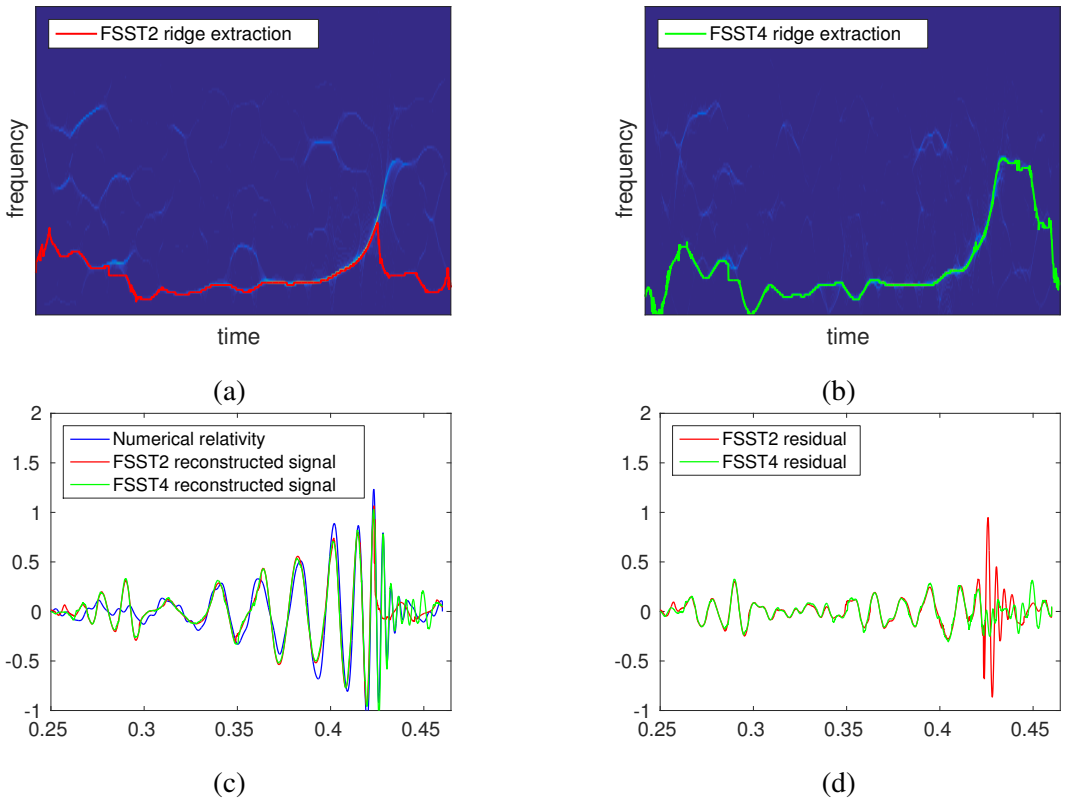

Fig. 8. (a): the ridge estimated from FSST2 displayed in Figure 7 (c); (b): same as (a) but on FSST4; (c): reconstructed signals along with numerical relativity waveform for a system with parameters consistent with those recovered from **GW150914** event confirmed by an independent computation; (d): their corresponding residuals after subtracting the numerical relativity waveform.

V. Conclusion

In this paper, we introduced a generalization of the short-time Fourier-based synchrosqueezing transform by defining new synchrosqueezing operators based on high order amplitude and phase approximations. Such a generalization allows us to better handle a wide variety of multicomponent signals containing very strongly modulated AM-FM modes. The interest of the proposed new technique was also demonstrated through numerical experiments both for simulated and real signals. Indeed, it successfully produces a TF picture more concentrated than other methods based on synchrosqueezing or reassignment, while allowing for a better invertibility of the TF representation. Future work should now be devoted to the theoretical analysis of the behavior of the proposed representations when applied to noisy signals, as was done in [9], [21] for the original FSST. In this regard, it would also be of interest to study the behavior of the transform when the type of noise is non Gaussian.

APPENDIX A
THE PROOF OF PROPOSITION III.1

Proof: First of all, we rewrite the expression (21) under matrix form:

$$\tilde{\omega}_f(t,\eta) = \mathbf{X}_N(t,\eta)\cdot\mathbf{R}_N(t)^T$$

where $\mathbf{Z}^T$ is the transpose of matrix $\mathbf{Z}$ and the two row vectors $\mathbf{X},\mathbf{R}$ defined as:

$$\mathbf{X}_N(t,\eta) = [1 \;\; x_{2,1}(t,\eta) \;\; ... \;\; x_{N,1}(t,\eta)]$$

$$\mathbf{R}_N(t) = [r_1(t) \;\; r_2(t) \;\; ... \;\; r_N(t)]$$

Let us denote $y_1 = \mathbf{X}_N\cdot\mathbf{R}_N^T$, we may thus write:

$$y_1 = \begin{bmatrix} x_{1,1} & x_{2,1} & x_{3,1} & \dots & x_{N,1}\end{bmatrix}\mathbf{R}_N^T. \tag{27}$$

It is noteworthy that $\Re\{r_1(t)\} = \phi'(t)$. To get r_k, we build up a system of N equations with variables r_k for $k = 1,\dots,N$ from (27) using the following procedure. By computing the partial derivatives of (27) with respect to η and using notation $y_2 = \dfrac{\partial_\eta y_1}{\partial_\eta x_{2,1}}$ and $x_{k,2} = \dfrac{\partial_\eta x_{k,1}}{\partial_\eta x_{2,1}}$, the second equation can be obtained:

$$y_2 = \begin{bmatrix} 0 & 1 & x_{3,2} & \dots & x_{N,2}\end{bmatrix}\mathbf{R}_N^T.$$

Doing the same thing iteratively, we can get the jth equation:

$$y_j = \begin{bmatrix} 0 & 0 & \dots & 1 & \dots & x_{N,j}\end{bmatrix}\mathbf{R}_N^T.$$

Combining all these equations, the desired system of equations can be deduced:

$$\begin{bmatrix} y_1 \\ y_2 \\ \vdots \\ y_{N-1} \\ y_N \end{bmatrix} = \begin{bmatrix} 1 & x_{2,1} & x_{3,1} & \dots & x_{N,1} \\ 0 & 1 & x_{3,2} & \dots & x_{N,2} \\ \vdots & \vdots & \ddots & \vdots & \vdots \\ 0 & 0 & 0 & \dots & x_{N,N-1} \\ 0 & 0 & 0 & \dots & 1 \end{bmatrix}\begin{bmatrix} r_1 \\ r_2 \\ \vdots \\ r_{N-1} \\ r_N \end{bmatrix}$$

or

$$\begin{bmatrix}\mathbf{Y}_N\end{bmatrix} = \begin{bmatrix}\mathbf{MX}\end{bmatrix}\begin{bmatrix}\mathbf{R}_N\end{bmatrix}^T. \tag{28}$$

Since $\mathbf{MX}$ is a upper triangular matrix with nonzero diagonal coefficients, we use back-substitution algorithm to get r_k for $k = 1,\dots,N$ as follows:

$r_N(t) = y_N(t,\eta)$ and

$$r_j(t) = y_j(t,\eta) - \sum_{k=j+1}^{N} x_{k,j}(t,\eta)r_k(t) \quad \text{for } j = N-1, N-2, \dots, 1.$$

As a result, $\tilde{q}_{\eta,f}^{[k,N]}(t,\eta) = r_k(t)$ for $k = 2,\ldots,N$. From (21), we clearly have: $\Re\left\{\tilde{q}_{\eta,f}^{[k,N]}(t,\eta)\right\} = \dfrac{\phi^{(k)}(t)}{(k-1)!}$ for $k = 2,\ldots,N$, which finishes the proof. ■

APPENDIX B
PROOF OF THE PROPOSITION III.3

Proof: By using $\partial_\eta V_f^{t^{k-1}g} = -i2\pi V_f^{t^k g}$ for $k \in \mathbb{N}$ and defining $X_{k,j} = V_f^g V_f^{t^k g} - V_f^{t^{j-1}g} V_f^{t^{k-j+1}g}$, we get the following formula:

$$\partial_\eta X_{k,j} = X_{k+1,j} + X_{k+1,j} - X_{k+1,2}.$$

Thus, the upper triangular part of matrix $\mathbf{MX}$ defined in (28) with $N = 4$ can be obtained as follows:

$$\begin{aligned}
x_{k,1} &= \frac{V_f^{t^{k-1}g}}{V_f^g} && \text{for } k = 1\ldots 4,\\
x_{k,2} &= \frac{\partial_\eta x_{k,1}}{\partial_\eta x_{2,1}} = \frac{V_f^g V_f^{t^k g} - V_f^{tg} V_f^{t^{k-1}g}}{V_f^g V_f^{t^2 g} - \left(V_f^{tg}\right)^2} = \frac{X_{k,2}}{X_{2,2}} && \text{for } k = 2\ldots 4,\\
x_{k,3} &= \frac{\partial_\eta x_{k,2}}{\partial_\eta x_{3,2}} = \frac{X_{k+1,3}X_{2,2} - X_{k,2}X_{3,3}}{X_{4,3}X_{2,2} - X_{3,2}X_{3,3}} && \text{for } k = 3\ldots 4,\\
x_{k,4} &= 1 && \text{for } k = 4
\end{aligned}$$

Also, the elements of vector $\mathbf{Y}$ are obtained by:

$$\begin{aligned}
y_1 &= \tilde{\omega}_f = \eta - \frac{1}{i2\pi}\frac{V_f^{g'}}{V_f^g},\\
y_2 &= \frac{\partial_\eta y_1}{\partial_\eta x_{2,1}}\\
&= \frac{1}{i2\pi}\frac{\left(V_f^g\right)^2 + V_f^g V_f^{tg'} - V_f^{tg} V_f^{g'}}{V_f^g V_f^{t^2 g} - \left(V_f^{tg}\right)^2} = \frac{W_2}{X_{2,2}}, \text{ with } W_2 = \frac{1}{i2\pi}\left[\left(V_f^g\right)^2 + V_f^g V_f^{tg'} - V_f^{tg} V_f^{g'}\right].\\
y_3 &= \frac{\partial_\eta y_2}{\partial_\eta x_{3,2}} = \frac{W_3 X_{2,2} - W_2 X_{3,3}}{X_{4,3}X_{2,2} - X_{3,2}X_{3,3}}, \text{ with } W_3 = \partial_\eta W_2.\\
y_4 &= \frac{\partial_\eta y_3}{\partial_\eta x_{4,4}} = \frac{\begin{array}{r}(X_{4,3}X_{2,2} - X_{3,2}X_{3,3})\, W_4\\ -\,(W_3 X_{2,2} - W_2 X_{3,3})\,(X_{5,4} + X_{5,3} - X_{5,2})\\ +\,(W_3 X_{3,2} - W_2 X_{4,3})\,(X_{4,4} + X_{4,3} - X_{4,2})\end{array}}{\begin{array}{r}(X_{4,3}X_{2,2} - X_{3,2}X_{3,3})\,(X_{6,4} + X_{6,3} - X_{6,2})\\ -\,(X_{5,3}X_{2,2} - X_{4,2}X_{3,3})\,(X_{5,4} + X_{5,3} - X_{5,2})\\ +\,(X_{5,3}X_{3,2} - X_{4,2}X_{4,3})\,(X_{4,4} + X_{4,3} - X_{4,2})\end{array}}, \text{ with } W_4 = \partial_\eta W_3.
\end{aligned}$$

With the help of back-substitution algorithm, the modulation operators read:

$$\tilde{q}_{\eta,f}^{[4,4]} = \frac{\begin{array}{r}(X_{4,3}X_{2,2} - X_{3,2}X_{3,3})\,W_4 \\ -\,(W_3X_{2,2} - W_2X_{3,3})\,(X_{5,4} + X_{5,3} - X_{5,2}) \\ +\,(W_3X_{3,2} - W_2X_{4,3})\,(X_{4,4} + X_{4,3} - X_{4,2})\end{array}}{\begin{array}{r}(X_{4,3}X_{2,2} - X_{3,2}X_{3,3})\,(X_{6,4} + X_{6,3} - X_{6,2}) \\ -\,(X_{5,3}X_{2,2} - X_{4,2}X_{3,3})\,(X_{5,4} + X_{5,3} - X_{5,2}) \\ +\,(X_{5,3}X_{3,2} - X_{4,2}X_{4,3})\,(X_{4,4} + X_{4,3} - X_{4,2})\end{array}}$$

$$\tilde{q}_{\eta,f}^{[3,4]} = \frac{W_3X_{2,2} - W_2X_{3,3}}{X_{4,3}X_{2,2} - X_{3,2}X_{3,3}} - \tilde{q}_{\eta,f}^{[4,4]}\frac{X_{5,3}X_{2,2} - X_{4,2}X_{3,3}}{X_{4,3}X_{2,2} - X_{3,2}X_{3,3}}$$

$$\tilde{q}_{\eta,f}^{[2,4]} = \frac{W_2}{X_{2,2}} - \tilde{q}_{\eta,f}^{[3,4]}\frac{X_{3,2}}{X_{2,2}} - \tilde{q}_{\eta,f}^{[4,4]}\frac{X_{4,2}}{X_{2,2}}.$$

Finally, we complete the proof of this proposition by using notation G_k and $G_{j,k}$ to rewrite the above expressions. ■

REFERENCES

[1] S. Meignen, T. Oberlin, and S. McLaughlin, "A new algorithm for multicomponent signals analysis based on synchrosqueezing: With an application to signal sampling and denoising," *IEEE Transactions on Signal Processing*, vol. 60, no. 11, pp. 5787–5798, 2012.

[2] Y. Y. Lin, H.-T. Wu, C. A. Hsu, P. C. Huang, Y. H. Huang, and Y. L. Lo, "Sleep apnea detection based on thoracic and abdominal movement signals of wearable piezo-electric bands," *IEEE Journal of Biomedical and Health Informatics*, 2016.

[3] C. L. Herry, M. Frasch, A. J. Seely, and H.-T. Wu, "Heart beat classification from single-lead ecg using the synchrosqueezing transform," *Physiological Measurement*, vol. 38, no. 2, pp. 171–187, 2017.

[4] K. Kodera, R. Gendrin, and C. Villedary, "Analysis of time-varying signals with small bt values," *IEEE Transactions on Acoustics, Speech, and Signal Processing*, vol. 26, no. 1, pp. 64–76, 1978.

[5] F. Auger and P. Flandrin, "Improving the readability of time-frequency and time-scale representations by the reassignment method," *IEEE Transactions on Signal Processing*, vol. 43, no. 5, pp. 1068–1089, 1995.

[6] I. Daubechies and S. Maes, "A nonlinear squeezing of the continuous wavelet transform based on auditory nerve models," *Wavelets in medicine and biology*, pp. 527–546, 1996.

[7] I. Daubechies, J. Lu, and H.-T. Wu, "Synchrosqueezed wavelet transforms: an empirical mode decomposition-like tool," *Applied and Computational Harmonic Analysis*, vol. 30, no. 2, pp. 243–261, 2011.

[8] G. Thakur and H.-T. Wu, "Synchrosqueezing-based recovery of instantaneous frequency from nonuniform samples." *SIAM J. Math. Analysis*, vol. 43, no. 5, pp. 2078–2095, 2011.

[9] G. Thakur, E. Brevdo, N. S. FučKar, and H.-T. Wu, "The synchrosqueezing algorithm for time-varying spectral analysis: Robustness properties and new paleoclimate applications," *Signal Processing*, vol. 93, no. 5, pp. 1079–1094, May 2013.

[10] M. Skolnik, *Radar Handbook*, Technology and Engineering, Eds. McGraw-Hill Education, 2008.

[11] J. W. Pitton, L. E. Atlas, and P. J. Loughlin, "Applications of positive time-frequency distributions to speech processing," *IEEE Transactions on Speech and Audio Processing*, vol. 2, no. 4, pp. 554–566, 1994.

[12] E. J. Candes, P. R. Charlton, and H. Helgason, "Detecting highly oscillatory signals by chirplet path pursuit," *Applied and Computational Harmonic Analysis*, vol. 24, no. 1, pp. 14–40, 2008.

[13] B. P. Abbott and al., "Observation of gravitational waves from a binary black hole merger," *Phys. Rev. Lett.*, vol. 116, 2016.

[14] T. Oberlin, S. Meignen, and V. Perrier, "Second-order synchrosqueezing transform or invertible reassignment? Towards ideal time-frequency representations," *IEEE Transactions on Signal Processing*, vol. 63, no. 5, pp. 1335–1344, March 2015.

[15] R. Behera, S. Meignen, and T. Oberlin, "Theoretical analysis of the second-order synchrosqueezing transform," *Applied and Computational Harmonic Analysis*, 2016.

[16] F. Auger, P. Flandrin, Y.-T. Lin, S. McLaughlin, S. Meignen, T. Oberlin, and H.-T. Wu, "Time-frequency reassignment and synchrosqueezing: An overview," *IEEE Signal Processing Magazine*, vol. 30, no. 6, pp. 32–41, 2013.

[17] R. Carmona, W. Hwang, and B. Torresani, "Characterization of signals by the ridges of their wavelet transforms," *IEEE Transactions on Signal Processing*, vol. 45, no. 10, pp. 2586–2590, Oct 1997.

[18] S. Meignen, D.-H. Pham, and S. McLaughlin, "On demodulation, ridge detection and synchrosqueezing for multicomponent signals," *IEEE Transactions on Signal Processing*, vol. 65, no. 8, pp. 2093–2103, 2017.

[19] L. Stanković, "A measure of some time–frequency distributions concentration," *Signal Processing*, vol. 81, no. 3, pp. 621–631, 2001.

[20] I. Daubechies, Y. G. Wang, and H.-T. Wu, "Conceft: concentration of frequency and time via a multitapered synchrosqueezed transform," *Philosophical Transactions of the Royal Society A: Mathematical, Physical and Engineering Sciences*, vol. 374, no. 2065, Mar 2016.

[21] H. Yang, "Statistical analysis of synchrosqueezed transforms," *Applied and Computational Harmonic Analysis*, Oct. 2017.